High-intensity polariton waves near the threshold for stimulated Brillouin scattering

L. V. Keldysh and S. G. Tikhodeev

P. N. Lebedev Institute of Physics and General Physics Institute, USSR Academy of Sciences
(Submitted 11 December 1985)
Zh. Eksp. Teor. Fiz. **90**, 1852–1870 (May 1986)

We investigate the interaction in a crystal between an intense coherent polariton wave, whose amplitude is close to the threshold for Mandelstam-Brillouin scattering, and a background of scattered-polariton "noise." Correlations between scattered polaritons and phonons emitted during this scattering are taken into account, leading to the creation of mixed phonon-polariton modes. Near threshold, the decay rate of one of these modes reduces to zero, and the number of quanta in the mode grows. Backscattering leads to the appearance of fluctuations in the forward waves, consisting of correlated polariton pairs. We describe the system using diagram techniques devised for nonequilibrium processes, and solve Dyson-type equations in the so-called τ-approximation, in which the usual polarization operators for polaritons and phonons do not depend on the amplitude of the coherent wave while the anomalous phonon-polariton polarization operator is linear in this amplitude. We show that near threshold the τ-approximation ceases to be useful, due to accumulation of quanta in the weakly-damped mode; this leads formally to an increase in the number of diagrams, along with an increase in the order of perturbation theory to which the phonon-polariton interaction must be treated. We show that this problem can be avoided if we include a large number of single-loop diagrams in the expressions for the polarization operators, in which case near threshold all "dressed" diagrams become first order (as in the theory of phase transitions); a full solution of the problem then requires use of the renormalization group. In this paper we set up a self-consistent approximation for treating a simplified one-dimensional system (for example, polaritons in an optical fiber), taking into account only the single-loop diagrams in the polarization operators.

INTRODUCTION

In this paper we will investigate the interaction between a coherent electromagnetic wave (i.e., a polariton) propagating in a crystal with frequency close to the polariton resonance and scattered-polariton "noise," in the case when the amplitude of the coherent wave is close to the threshold for stimulated Mandelstam-Brillouin scattering. In this situation, the intensity of the noise is found to increase strongly, and the "feedback effect" of this noise on the propagation of the coherent wave becomes appreciable. In addition, this effect also gives rise to a significant modification in the spectra both of the scattered polaritons and of the propagating waves. The fact that polariton-acoustic phonon scattering accompanies each scattering event leads to the appearance of a certain coherence between polaritons and phonons. As a result, in place of the original polariton-phonon scattering there appear mixed polariton-phonon modes, just as the photon-exciton interaction gives rise to the polaritons themselves. Near the threshold for stimulated scattering, the decay constant of one of these mixed modes goes to zero; hence, there is an accumulation of quanta in this mode, and the intensity of the mode increases strongly. Under these conditions, the behavior both of the scattered polaritons and the phonons in resonance with them is entirely determined by only one of these weakly-damped modes, so that in practice the scattered polaritons and phonons behave as practically identical particles. The scattering process we investigate here is in effect transformed into one in which a coherent polariton wave decays into two practically identical "mixed" particles. The feedback effect of these scattered particles on the original wave (i.e., back-scattering) leads to the development of intense fluctuations around it, whose spectral width increases as threshold is approached. In polariton language, these fluctuations correspond to polariton pairs whose frequencies and propagation directions are close to the original wave; these pairs arise as a consequence of the intense interaction and secondary scattering of the weakly-damped mixed phonon-polariton modes.

The formal investigation of the physical picture described above is carried out here within the framework of the diagram theory of nonequilibrium processes. For simplicity, the amplitude of the coherent wave is taken to be given, and depends neither on time nor on the coordinates. From a formal point of view, this is equivalent to assuming there is in the medium a distribution of internal sources when sustain this amplitude despite the losses connected with scattering. From the standpoint of physics, this limits the region of applicability of the results we obtain to fields not too close to threshold, for which the intensity of the scattered waves is still small compared to the forward wave, which can therefore be treated approximately as a given "pump." The relevant quantitative criteria will be presented at the end of the article.

In section 1 we formulate rules for the diagram technique, and obtain and solve the equations for the normal

 0038-5646/86/051086-11$04.00

phonon and polariton propagators, the anomalous propagators for correlated phonons and scattered polaritons, and correlated pairs of forward polaritons.

In section 2 we develop the so-called τ-approximation, in which we take into account only low-order terms (not the linear terms mentioned above) in the expansion of the polarization operator in powers of the amplitude of the coherent wave. Within the framework of the τ-approximation we investigate the poles of the Green's function for polaritons which scatter with phonon emission (i.e., the Stokes component of the scattered-polariton spectrum) and for resonance phonons. The analogous problem for the anti-Stokes component was solved in Ref. 1. It is shown that when a certain threshold value of the intensity of the forward wave is attained, the decay constant of one of the mixed phonon-polariton modes changes sign, i.e., stimulated polariton scattering occurs.

In section 3, we investigate the properties of a system near the threshold for stimulated scattering. It is shown that the normal and anomalous propagators for scattered polaritons and phonons near threshold grow (which corresponds to the decrease in the decay constant of one of the mixed modes and the accumulation of quanta in it). Near the threshold, the τ-approximation is found to be inadequate; diagrams which are not taken into account in this approximation for the polarization operator of forward polaritons diverge as threshold is approached. Furthermore, the number of diagrams grows with increasing orders of perturbation theory. This latter difficulty can be overcome if we go beyond the τ-approximation framework and include in the forward-polariton polarization operator the single-loop diagrams, which are very large near threshold. Then the leading diagrams cancel out, and the order of the diagrams does not grow as the order of perturbation theory increases. Consequently, the situation near threshold for stimulated scattering is similar to the situation near a phase transition, and a full solution to the problem requires the use of the renormalization group.

In section 4 we construct a simplified model in which quanta of the coherent mode decay into pairs of quanta with the same free-particle spectrum. In addition, we investigate a one-dimensional system (for example, polariton waves in an optical fiber).

In sections 5 and 6, we set up a self-consistent approximation for the model system near threshold, analogous to the mean-field approximation—including one-loop diagrams for the polarization operator. It is shown that broad-spectrum, low-intensity fluctuations arise near the forward wave. This noisy component near the coherent wave gives rise to an essential change in the lifetime and occupation number of the scattered particles.

In conclusion, we analyze the applicability of the one-dimensional self-consistent approximation to a system of polaritons in an optical fiber.

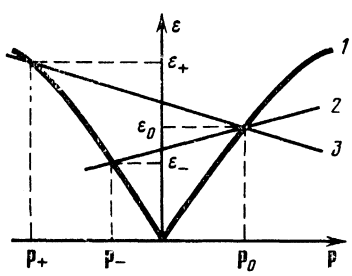

FIG. 1. Polariton branch (1) along with the absorption (2) and emission (3) spectra of phonons. The intersection of the dispersion manifolds with a plane passing through the vector p is shown.

1. SCATTERING OF POLARITONS IN A COHERENT MACROSCOPICALLY-OCCUPIED MODE OFF OF PHONONS: POINT OF VIEW

Let us investigate the interaction between a large-amplitude electromagnetic wave in a direct-gap semiconductor and acoustic phonons. As is well-known,[2] the exciton-photon interaction in direct-gap semiconductors leads to renormalization of the exciton and photon spectra, i.e., to the appearance of polariton branches. We will assume that this renormalization has already been included in the free-particle Hamiltonians for polaritons and phonons. We will treat the influence of the large-amplitude electromagnetic wave by assuming that one of the polariton modes is macroscopically occupied (i.e., its occupation number is large and proportional to the system volume), and furthermore that the mode is in a coherent state. Let $p_0 = (\varepsilon_0, \mathbf{p}_0)$ be the frequency and wave vector of this mode [here $\varepsilon_0 = \varepsilon(\mathbf{p}_0)$, and $\varepsilon(\mathbf{p})$ is the dispersion relation for the polariton]. Then the scattering of polaritons out of this mode with absorption and emission of phonons will also populate other polariton modes. We estimate their characteristic frequency and wave vector $p_\pm = (\varepsilon_\pm, \mathbf{p}_\pm)$ where the index " + " refers to absorption and " − " to emission of a phonon. Let us note that the matrix element for interaction with acoustic phonons grows with the momentum transfer, and is a maximum for backward scattering (see Fig. 1). We therefore take as a characteristic energy of the scattered polaritons the quantities $\varepsilon_\pm = \varepsilon(\mathbf{p}_\pm)$, where the $\mathbf{p}_\pm$, i.e., the characteristic momenta of the scattered polaritons, are solutions to the equation

$$\varepsilon(\mathbf{p}_0) = \varepsilon(\mathbf{p}_\pm) \pm u|\mathbf{p}_\pm - \mathbf{p}_0|, \tag{1.1}$$

while u is the velocity of sound. The characteristic frequencies and momenta of the phonons are $p_\pm - p_0$. Since $p_\pm$ differ significantly from p_0, the back-scattered polaritons and forward-scattered polaritons are quanta of essentially different kinds. We will underline this state of affairs by using different notations for polariton propagators with $p \sim p_0$ and $p \sim p_\pm$. Because of this notational convention, the results we derive below are applicable to any three-quantum process in which a coherent macroscopically-occupied mode takes part.

In order to describe the system, we will make use of the diagram technique for nonequilibrium processes,[3] in which particle propagators are matrices with temporal indices i, $j = 1, 2$. In applying perturbation theory to the polariton-phonon interaction, we consider only "resonance" diagrams in which the coherent-mode polariton takes part, along with the neighboring modes with $p \sim p_0$, the scattered polaritons with $p \sim p_\pm$ and phonons with $k \sim p_0 - p_\pm$. Measuring fre-

quencies and momenta of these particles from $p_0, p_\pm$, and $p_0 - p_\pm$, we can display their free-particle Green's functions in the forms

$$D_0(p)=\begin{pmatrix} 0 & D_0^a \\ D_0^r & S_0 \end{pmatrix}=\begin{pmatrix} 0 & [\varepsilon-\varepsilon_0(\mathbf{p})-i0]^{-1} \\ [\varepsilon-\varepsilon_0(\mathbf{p})+i0]^{-1} & -2\pi i\delta[\varepsilon-\varepsilon_0(\mathbf{p})] \end{pmatrix}, \tag{1.2}$$

$$G_{0,pol}(p)=\begin{pmatrix} 0 & G_{0,pol}^a \\ G_{0,pol}^r & F_{0,pol} \end{pmatrix}$$

$$=\begin{pmatrix} 0 & [\varepsilon-\varepsilon_\pm(\mathbf{p})-i0]^{-1} \\ [\varepsilon-\varepsilon_\pm(\mathbf{p})+i0]^{-1} & -2\pi i\delta[\varepsilon-\varepsilon_\pm(\mathbf{p})] \end{pmatrix} \tag{1.3}$$

$$G_{0,ph}(p)=\begin{pmatrix} 0 & G_{0,ph} \\ G_{0,ph}^r & F_{0,ph} \end{pmatrix}$$

$$=\begin{pmatrix} 0 & \mp[\varepsilon-\omega_\pm(\mathbf{p})-i0]^{-1} \\ \mp[\varepsilon-\omega_\pm(\mathbf{p})+i0]^{-1} & -2\pi i(1+2N_\pm)\delta(\varepsilon-\omega_\pm) \end{pmatrix} \tag{1.4}$$

where

$$p=(\varepsilon, \mathbf{p}),\quad \varepsilon_\alpha(\mathbf{p})=\varepsilon(\mathbf{p}+\mathbf{p}_\alpha)-\varepsilon_\alpha,$$

$$\alpha=0, +, -,\ \omega_\pm(\mathbf{p})=\mp u|\mathbf{p}+\mathbf{p}_0-\mathbf{p}_\pm|+\varepsilon_\pm-\varepsilon_0,$$

$$N_\pm=[\exp(\hbar u|\mathbf{p}_0-\mathbf{p}_\pm|/k_BT)-1]^{-1},$$

and $N_\pm$ is the phonon number density in thermal equilibrium. We have assumed that the temperature is small compared to ε_α/k_B, and that we can neglect the polaritons as a heat source. In order to derive (1.4) from the expressions usually used (see e.g., Ref. 3), we have taken the positive-frequency part for phonon emission and the negative-frequency part for phonon absorption. The indices " $\pm$ " on the Green's functions $G_{0,\alpha}$ are not written explicitly, since in the resonance approximation the contributions of absorbed and emitted phonons cannot be confused, and can be computed separately.

Let us denote the matrix D_0 graphically by a wavy line (Fig. 2a), $G_{0,\text{pol}}$ by a straight line (Fig. 2b), and $G_{0,\text{ph}}$ by a dashed line (Fig. 2c). The interaction of polaritons and phonons in the deformation-potential approximation corresponds to the vertices in Fig. 2d. The point in the figures represents the matrix vertex function with temporal indices $i, j, l = 1, 2$:

$$i^{1/2}\mu_{\mathbf{k}}M_{ij}^{\ l}(2\pi)^4\delta(p-k-p'), \tag{1.5}$$

where

$$\mu_{\mathbf{k}}=\tfrac{1}{2}D(|\mathbf{k}-\mathbf{p}_\pm+\mathbf{p}_0|/\hbar\rho u)^{1/2},\qquad M_{ij}^{\ l}=\delta_{1,l}\delta_{i,j}+\delta_{2,l}(\sigma_x)_{ij}, \tag{1.6}$$

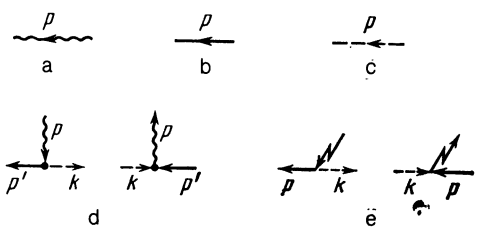

FIG. 2. The free Green's functions D_0 (a), $G_{0,\text{pol}}$ (b), $G_{0,\text{ph}}$ (c), the normal vertices for the polariton-phonon interaction (d) and the anomalous vertices (e).

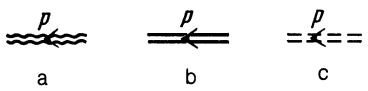

FIG. 3. Green's functions D (a), G_{pol} (b) and G_{ph} (c).

here, D is the polariton deformation potential constant, ρ is the semiconductor density, and σ_x is the first Pauli matrix.

Our treatment of the effect of the coherent mode with $p = p_0$ parallels the treatment of such modes in the diagrammatic analysis of Bose systems,[4] i.e., we add new vertices (of external-field type, see Fig. 2e) which consist of matrices with temporal indices $i, j = 1, 2$:

$$\Phi_{ij}(p)=\Phi_{\mathbf{p}}(2\pi)^4\delta(k+p)\,(\sigma_x)_{ij}, \tag{1.7}$$

where

$$\Phi_{\mathbf{p}}=\mu_{-\mathbf{p}}(2n_0)^{1/2}=D(n_0|\mathbf{p}+\mathbf{p}_\pm-\mathbf{p}_0|/2\hbar\rho u)^{1/2},$$

n_0 is the spatial density of polaritons in the coherent mode, which we take as an externally-imposed parameter. Likewise, in determining the anomalous vertices corresponding to creation and annihilation of polaritons, we have fixed the phase of the coherent wave at $\varphi = 0$. This is legitimate, since later on we will be interested in stationary solutions which do not depend on the phase.

For a full description of the system, i.e., one which takes into account the anomalous vertices (1.7), in addition to the exact Green's functions for polaritons with $p \sim p_0$ (Fig. 3a):

$$D(p)=\begin{pmatrix} 0 & D^a \\ D^r & S \end{pmatrix}, \tag{1.8}$$

for scattered polaritons (α = pol, Fig. 3b) and for phonons (α = ph, Fig. 3c):

$$G_\alpha(p)=\begin{pmatrix} 0 & G_\alpha^a \\ G_\alpha^r & F_\alpha \end{pmatrix}, \tag{1.9}$$

we need to introduce anomalous propagators. For scattered polaritons and phonons, we call these functions $G_\diamond(p, -p)$ and $G_\times(-p, p)$ (Figs. 4a and 4b); they are proportional respectively to $\langle T_c ab\rangle$ and $\langle T_c a^+ b^+\rangle$, where a^+ and b^+ are creation operators for a polariton and a phonon. For polaritons with $p \sim p_0$, we use the Beliaev functions $D_\diamond(p, -p)$ and $D_\times(-p, p)$ (Figs. 4c and 4d), corresponding to creation of polariton pairs out of the Bose-condensate and to annihilation of such pairs. We will use a notation analogous

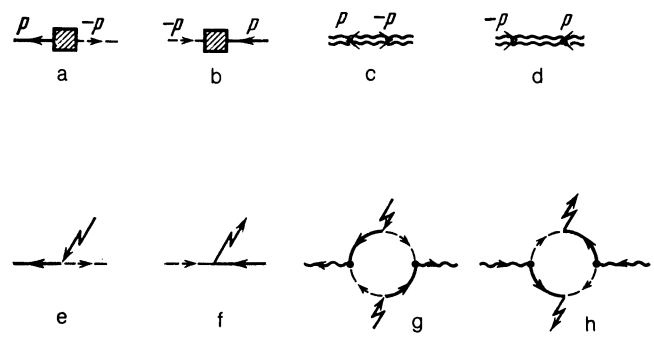

FIG. 4. Anomalous functions $G_\diamond$ (a), $\overline{G}_\times$ (b), $D_\diamond$ (c), $\overline{D}_\times$ (d) and the simplest diagrams which correspond to them in (e–h).

to (1.8) and (1.9) for the time components of these functions. The simplest diagrams for the anomalous propagators are shown in Figs. 4e–4h. Further on, we will use the abbreviated notation $G_\alpha \equiv G_\alpha(p)$, $\overline{G}_\alpha \equiv G_\alpha(-p)$, $G_\diamond \equiv G_\diamond(p,-p)$, and $\overline{G}_\times \equiv G_\times(-p,p)$, etc., when this will not lead to confusion.

It is convenient to combine these functions, which are all matrices in the temporal indices, into matrices $g_{\alpha\beta}(p)$, $d_{\alpha\beta}(p)$, $\alpha,\beta = 1,2$:

$$g(p)=\begin{bmatrix} G_{pol} & G_\diamond \\ \overline{G}_\times & \overline{G}^T_{ph} \end{bmatrix}, \quad d(p)=\begin{bmatrix} D_\diamond & D \\ \overline{D}^T & \overline{D}_\times \end{bmatrix}, \tag{1.10}$$

where "T" denotes the transpose of a matrix. Let us also take

$$g_0(p)=\begin{bmatrix} G_{0,pol} & 0 \\ 0 & \overline{G}^T_{0,ph} \end{bmatrix}, \quad d_0(p)=\begin{bmatrix} 0 & D_0 \\ \overline{D}_0{}^T & 0 \end{bmatrix}. \tag{1.11}$$

Let us emphasize that the matrices (1.10) and (1.11) are four-rowed matrices, since the quantities $G_{\rm pol}$, etc., are themselves two-rowed matrices in the temporal indices. From here on we will denote matrices of this kind with lower case letters. The extra indices, i.e., the nontemporal ones, we will refer to as "external" indices and denote by Greek letters. On the graph, we will denote the matrices corresponding to the lines with large black arrows (see Fig. 5).

It is easy to see that any diagram for the Green's functions (1.8), (1.9) etc., can be obtained as a matrix component of the topologically-equivalent graphs for the functions (1.10), in which the propagators D_0 and $G_{0,\alpha}$ are replaced by the matrices (1.11), while the vertex matrix (the triangle in the diagrams in Fig. 5e)

$$i^{1/2}\mu_k m_{\alpha\beta}{}^\gamma = i^{1/2}\mu_k \delta_{\alpha,\gamma}(\sigma_x)_{\gamma\beta} \otimes M_{ij}{}^k \tag{1.12}$$

has only two non-zero components m^1_{12} and m^2_{21}.

Let us introduce the polarization operators, which consist of sums of all single-particle operators of a given type. We require polarization operators for scattered polaritons ($\alpha = $ pol), phonons ($\alpha = $ ph) and polaritons with $p \sim p_0$:

$$\Sigma_\alpha(p)=\begin{pmatrix} \Omega_\alpha & \Sigma_\alpha{}^r \\ \Sigma_\alpha{}^a & 0 \end{pmatrix}, \quad \Pi_{11}(p)=\begin{pmatrix} \Delta_{11} & \Pi_{11}{}^r \\ \Pi_{11}{}^a & 0 \end{pmatrix}, \tag{1.13}$$

as well as the anomalous operators for creation and annihilation of phonons and scattered polaritons $\Sigma_{02}(p,-p)$ and $\Sigma_{20}(-p,p)$ and also for creation and annihilation of pairs of $p \sim p_0$ polaritons: $\Pi_{02}(p,-p)$ and $\Pi_{20}(-p,p)$.[1)] The simplest diagrams for Σ_{02} and Σ_{20} consist of the vertices

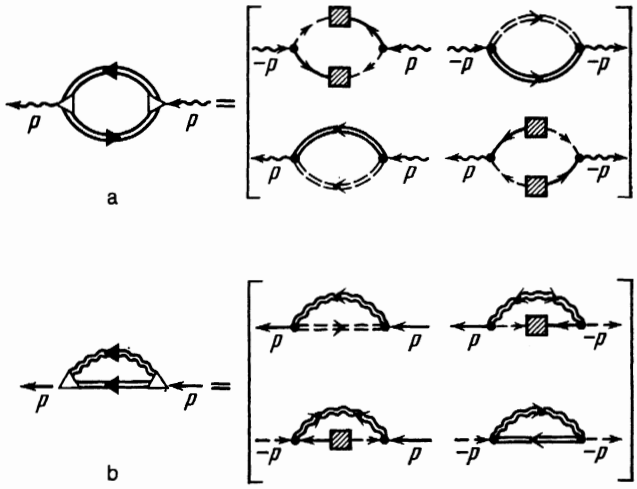

FIG. 6. Diagrams for the polarization operators for polaritons with $p \sim p_0$ (a), and scattered polaritons and phonons (b).

(1.7), i.e., linear in $n_0^{1/2}$ (or Φ). It is convenient to treat them separately, beginning with an expansion of Σ_{02} and Σ_{20} to third order in $n_0^{1/2}$. The simplest diagrams for Π_{02} and Π_{20} appear in the central blocks of Figs. 4g and 4h.

Let us combine the polarization operators into two matrices $\sigma_{\alpha\beta}$ and $\pi_{\alpha\beta}$:

$$\sigma(p)=\begin{bmatrix} \Sigma_{pol} & \Sigma_{02} \\ \Sigma_{20} & \Sigma_{ph}{}^r \end{bmatrix}, \quad \pi(p)=\begin{bmatrix} \Pi_{20} & \Pi_{11}{}^r \\ \Pi_{11} & \Pi_{02} \end{bmatrix}. \tag{1.14}$$

The simplest skeleton diagrams for these operators and their matrix components are shown in Fig. 6.

In addition, let

$$\varphi(p)=\begin{bmatrix} 0 & \Phi(p) \\ \Phi(p) & 0 \end{bmatrix}. \tag{1.15}$$

We obtain the standard equations for the functions (1.10):

$$g = g_0 + g_0(\sigma+\varphi)g, \tag{1.16}$$

$$d = d_0 + d_0\pi d. \tag{1.17}$$

The structure of these equations for the various matrix components is shown in Fig. 7. It is easy to obtain the solutions to (1.16), (1.17) for the leading-order Green's functions:

$$g^a(p) \equiv \begin{bmatrix} G^a_{pol} & G_\diamond{}^a \\ \overline{G}_\times{}^a & \overline{G}^r_{ph} \end{bmatrix} = \frac{1}{Z^a(p)}\begin{bmatrix} \overline{G}^{-1}_{0,ph} - \overline{\Sigma}^r_{ph} & \overline{\Sigma}^a_{20} + \Phi \\ \Sigma_{02}{}^a + \Phi & G^{-1}_{0,pol} - \Sigma^a_{pol} \end{bmatrix}, \tag{1.18}$$

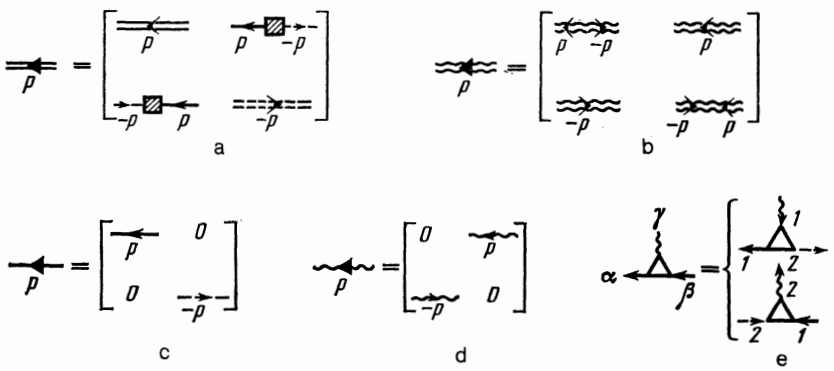

FIG. 5. Graphical notation for the matrices g, d, g_0, d_0, $i^{1/2}\mu m^\gamma_{\alpha\beta}$ along with their matrix structure.

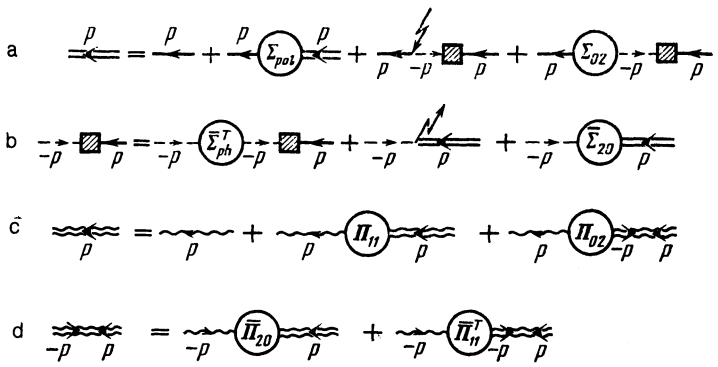

FIG. 7. Equations (1.16) and (1.17) for the components G_{pol} (a), $\bar{G}_\times$ (b), D (c) and $\bar{D}_\times$ (d).

$$d^a(p)\equiv\begin{bmatrix} D_\Diamond{}^a & D^a \\ \bar{D}^r & \bar{D}_\times{}^a \end{bmatrix}=\frac{1}{Y^a(p)}\begin{bmatrix} \Pi_{02}{}^a & \bar{D}_0^{-1}-\bar{\Pi}_{11}{}^r \\ D_0^{-1}-\Pi_{11}{}^a & \bar{\Pi}_{20}{}^a \end{bmatrix}, \tag{1.19}$$

where

$$G_{0,pol}^{-1}(p)=\varepsilon-\varepsilon_\pm(\mathbf{p}),\quad \bar{G}_{0,ph}^{-1}\equiv G_{0,ph}^{-1}(-p)=\pm[\varepsilon+\omega_\pm(-\mathbf{p})],$$

$$D_0{}^{-1}=\varepsilon-\varepsilon_0(\mathbf{p}),$$

$$Z^a(p)=[\bar{G}_{0,ph}^{-1}-\Sigma_{ph}{}^r][G_{0,pol}^{-1}-\Sigma_{pol}^a]-[\Sigma_{20}+\Phi][\Sigma_{02}+\Phi], \tag{1.20}$$

$$Y^a(p)=[\bar{D}_0{}^{-1}-\bar{\Pi}_{11}{}^r]\,[D_0{}^{-1}-\Pi_{11}{}^a]-\Pi_{02}{}^a\bar{\Pi}_{20}{}^a. \tag{1.21}$$

A more cumbersome expression for the static Green's functions can be found using the matrix formulae

$$f=g^r\omega g^a,\quad s=d^r\delta d^a, \tag{1.22}$$

where

$$f_\Lambda^\nu=\begin{bmatrix} F_{pol} & F_\Diamond \\ \bar{F}_\times & \bar{F}_{ph} \end{bmatrix},\quad \omega=\begin{bmatrix} \Omega_{pol} & \Omega_{02} \\ \bar{\Omega}_{20} & \bar{\Omega}_{ph} \end{bmatrix},$$

$$s=\begin{bmatrix} S_\Diamond, S \\ \bar{S} & \bar{S}_\times \end{bmatrix},\quad \delta=\begin{bmatrix} \bar{\Delta}_{20} & \bar{\Delta}_{11} \\ \Delta_{11} & \Delta_{02} \end{bmatrix}. \tag{1.23}$$

Formula (1.22) follows from (1.16) and (1.17), and is analogous to the formula $F=G^r\Omega G^a$,[3] which is correct in the absence of anomalous Green's functions. For example,

$$F_{pol}=G_{pol}^r[\Omega_{pol}G_{pol}^a+\Omega_{02}\bar{G}_\times{}^a]+G_\Diamond{}^r[\bar{\Omega}_{ph}\bar{G}_\times{}^a+\bar{\Omega}_{20}G_{pol}^a]. \tag{1.24}$$

2. THE τ-APPROXIMATION: QUASIPARTICLE (PHONORITON) SPECTRUM

Let us first consider only the lowest-order diagrams in power of $n_0^{1/2}$ (no higher than linear) for the polarization operators. In this approximation, which we call henceforth the τ-approximation, the normal polarization operators do not depend on Φ, while the anomalous ones, whose expansion in powers of Φ begins with quadratic (for Π_{02}, Π_{20}) and cubic (for Σ_{02}, Σ_{20}) terms, equal zero.

Near the corresponding surfaces $\varepsilon=\varepsilon(p)$, in the τ-approximation $\Sigma_\alpha(p)$ and $\Pi_{11}(p)$ can be expressed in terms of the polariton lifetime $\tau_{\text{pol}}(\mathbf{p})=\gamma_{\text{po}}^{-1}(\mathbf{p})$ and phonon lifetime $\tau_{\text{ph}}=\gamma_{\text{ph}}^{-1}$ (see, e.g., Ref. 5):

$$\Sigma_{pol}=i\gamma_{pol}\begin{pmatrix} -2 & -1 \\ 1 & 0 \end{pmatrix},\quad \Pi_{11}=i\gamma_{pol}^0\begin{pmatrix} -2 & -1 \\ 1 & 0 \end{pmatrix}, \tag{2.1}$$

$$\Sigma_{ph}=i\gamma_{ph}\begin{pmatrix} -2(1+2N_\pm) & \mp 1 \\ \pm 1 & 0 \end{pmatrix}. \tag{2.2}$$

Here the upper sign, as before, refers to absorption of phonons, the lower one to emission. The solution to (1.17) is trivial:

$$D(p)=\begin{pmatrix} 0 & [\varepsilon-\varepsilon_0(\mathbf{p})-i\gamma_{pol}^0]^{-1} \\ [\varepsilon-\varepsilon_0(\mathbf{p})+i\gamma_{pol}^0]^{-1} & \dfrac{-2\pi i\gamma_{pol}^0}{[\varepsilon-\varepsilon_0(\mathbf{p})]^2+[\gamma_{pol}^0]^2} \end{pmatrix}, \tag{2.3}$$

$$D_\Diamond=D_\times=0, \tag{2.4}$$

and the quantity which replaces the functions $G_{\text{pol}}^a,\ldots$ equals

$$Z^a(p)=[\bar{G}_{0,ph}^{-1}-\Sigma_{ph}{}^r][G_{0,pol}^{-1}-\Sigma_{pol}^a]-\Phi_p{}^2. \tag{2.5}$$

Let us investigate the zeroes of the function (2.5). We obtain a quadratic for the excitation spectrum:

$$[\pm\varepsilon\pm\omega_\pm(-\mathbf{p})\mp i\gamma_{ph}]\,[\varepsilon-\varepsilon_\pm(\mathbf{p})-i\gamma_{pol}]-\Phi_p{}^2=0. \tag{2.6}$$

The behavior of the solutions (2.6) for the anti-Stokes component (the upper sign in 2.6) was analyzed in Ref. 1; we therefore limit ourselves to an analysis of the Stokes component. The two solutions to (2.6), which (following Ref. 1) we will call "phonoritons," take the form

$$\varepsilon_{1,2}(\mathbf{p})={}^1/_2\{\varepsilon_-(\mathbf{p})-\omega_-(-\mathbf{p})+i\Gamma$$

$$\pm([\varepsilon_-(\mathbf{p})+\omega_-(-\mathbf{p})+i\gamma]^2-4\Phi_p{}^2)^{1/2}\}, \tag{2.7}$$

where $\Gamma=\gamma_{\text{ph}}+\gamma_{\text{pol}}$, $\gamma=\gamma_{\text{pol}}-\gamma_{\text{ph}}$. Separating out the real and imaginary parts of (2.7),[2)] we obtain

$$\operatorname{Re}\varepsilon_{1,2}(\mathbf{p})={}^1/_2\{\varepsilon_-(\mathbf{p})-\omega_-(-\mathbf{p})$$

$$\pm 2^{-1/2}[(Q_p{}^2+R_p{}^2)^{1/2}+Q_p]^{1/2}\operatorname{sgn}R_p\}, \tag{2.8}$$

$$\operatorname{Im}\varepsilon_{1,2}(\mathbf{p})={}^1/_2\{\Gamma\pm 2^{-1/2}[(Q_p{}^2+R_p{}^2)^{1/2}-Q_p]^{1/2}\}, \tag{2.9}$$

where

$$Q_p=[\varepsilon_-(\mathbf{p})+\omega_-(-\mathbf{p})]^2-\gamma^2-4\Phi_p{}^2,$$

$$R_p=2[\varepsilon_-(\mathbf{p})+\omega_-(-\mathbf{p})]\gamma. \tag{2.10}$$

In certain ranges of momentum the decay constant of one of the phonoritons can change sign ($\operatorname{Im}\varepsilon_2<0$). Over

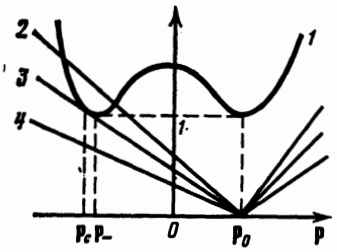

FIG. 8. Graphical solution to equation (2.11); the figure is explained in the text.

these ranges of p, it is possible to generate polaritons and phonons; therefore, the stationary approximation is meaningful only in the region below threshold.

From (2.9), it follows that the boundary surface in momentum space which satisfies the condition $\operatorname{Im}\varepsilon_2 = 0$ is given by the equation

$$1+[\varepsilon_-(\mathbf{p})+\omega_-(-\mathbf{p})]^2/\Gamma^2=\Phi_{\mathbf{p}}^2/\bar{\gamma}^2, \tag{2.11}$$

where $\bar{\gamma} = (\gamma_{\text{pol}}\gamma_{\text{ph}})^{1/2}$. The properties of equation (2.11) are illustrated in Fig. 8, in which curve 1 shows the dependence of the left side of (2.11) on longitudinal momentum $p_\parallel = \mathbf{p}_0\cdot\mathbf{p}$ for $p_\perp = 0$. Curves 2–4 give the dependence of the right side of (2.11) on $p_\parallel$ for various coherent-mode densities. If the density is smaller than a certain critical value, i.e., $n_0 < n_c$ (curve 4), equation (2.11) has no solution and both phonoriton branches are stable. For $n_0 = n_c$ (curve 3), $\operatorname{Im}\varepsilon_2 > 0$ everywhere, excluding the tangent point $p = p_c$, at which $\operatorname{Im}\varepsilon_2 = 0$. For $n_0 > n_c$ (curve 2) there is a region of momenta around p in which $\operatorname{Im}\varepsilon_2 < 0$ and stimulated polariton scattering can occur. It is not hard to show that to within small terms of order $(\Gamma/\varepsilon_0)^2 \ll 1$

$$\mathbf{p}_c \approx \mathbf{p}_-. \tag{2.12}$$

Therefore

$$n_c \approx 2\bar{\gamma}^2\hbar\rho u/D^2|\mathbf{p}_- - \mathbf{p}_0|, \qquad \Phi|_{\mathbf{p}=0,\ n_0=n_c} \approx \bar{\gamma}. \tag{2.13}$$

In Fig. 9 we illustrate schematically the functions $\operatorname{Re}\varepsilon_{1,2}$ (2.18) and $\operatorname{Im}\varepsilon_{1,2}$ (2.9) for $n_0 = n_c$.

3. ABOVE-THRESHOLD REGION: INADEQUACY OF THE τ-APPROXIMATION

Fundamental interest attaches to an investigation of the Green's functions (1.18), (1.22) in the region near threshold—for $n_0 = n_c(1-\lambda)$, $0 < \lambda \ll 1$—and in a small region of frequency and momentum around p_-. In this case

$$\Phi_{\mathbf{p}}^2 \approx \bar{\gamma}^2(1-\lambda)|\mathbf{p}+\mathbf{p}_- - \mathbf{p}_0|/|\mathbf{p}_- - \mathbf{p}_0|. \tag{3.1}$$

Saving the leading terms in an expansion in $\lambda \ll 1$, we obtain

$$\operatorname{Im}\varepsilon_1(\mathbf{p}) \approx \Gamma, \tag{3.2}$$

$$\operatorname{Im}\varepsilon_2(\mathbf{p}) \approx (\bar{\gamma}^2/\Gamma)(\lambda + ap_\parallel^2 + bp_\perp^2), \tag{3.3}$$

$$\operatorname{Re}\varepsilon_1(\mathbf{p}) = \varepsilon_-(\mathbf{p})\gamma_{pol}/\Gamma - \omega_-(-\mathbf{p})\gamma_{ph}/\Gamma \approx -u_1 p_\parallel + v_1 p_\perp^2/2|\mathbf{p}_0|, \tag{3.4}$$

$$\operatorname{Re}\varepsilon_2(\mathbf{p}) = \varepsilon_-(\mathbf{p})\gamma_{ph}/\Gamma - \omega_-(-\mathbf{p})\gamma_{pol}/\Gamma \approx -u_2 p_\parallel + v_2 p_\perp^2/2|\mathbf{p}_0|, \tag{3.5}$$

where

$$a = \left(\frac{c+u}{\Gamma}\right)^2, \quad b = \frac{(c+u)^2}{8(c-u)c|\mathbf{p}_0|^2}, \quad c = \left|\frac{\partial\varepsilon(\mathbf{p})}{\partial\mathbf{p}}\right|_{\mathbf{p}=\mathbf{p}_-},$$
$$u_{1(2)} = c\gamma_{pol(ph)}/\Gamma - u\gamma_{ph(pol)}/\Gamma,$$
$$v_{1(2)} = c\frac{c+u}{c-u}\frac{\gamma_{pol(ph)}}{\Gamma} - u\frac{c+u}{2c}\frac{\gamma_{ph(pol)}}{\Gamma}. \tag{3.6}$$

In the Green's function (1.18) we can ignore the pole with $\varepsilon = \varepsilon_1(p)$ in view of the large damping of $\operatorname{Im}\varepsilon_1$ compared to $\operatorname{Im}\varepsilon_2$ (see Fig. 9b). Let

$$\varkappa_{\mathbf{p}} = -u_2 p_\parallel + v_2 p_\perp^2/2|\mathbf{p}_0| + i(\bar{\gamma}^2/\Gamma)(\lambda + ap_\parallel^2 + bp_\perp^2). \tag{3.7}$$

Then to the same accuracy as (3.2)–(3.5), we obtain

$$g(p) = \begin{bmatrix} (\gamma_{ph}/\Gamma)R(p) & i(\bar{\gamma}/\Gamma)R(p)\sigma_z \\ -i(\bar{\gamma}/\Gamma)\sigma_z R(p) & (\gamma_{pol}/\Gamma)\sigma_z R(p)\sigma_z \end{bmatrix}, \tag{3.8}$$

where

$$R(p) = \begin{pmatrix} 0 & (\varepsilon - \varkappa_{\mathbf{p}})^{-1} \\ (\varepsilon - \varkappa_{\mathbf{p}}^*)^{-1} & -4i\dfrac{\bar{\gamma}^2(1+N_-)}{\Gamma|\varepsilon - \varkappa_{\mathbf{p}}|^2} \end{pmatrix}. \tag{3.9}$$

For small $p^{(3)}$ (for $|\varepsilon| \lesssim \bar{\gamma}^2\lambda/\Gamma$; $|\mathbf{p}| \lesssim \Gamma\lambda^{1/2}/c$), the components $R(p)$ of (3.9) are large: the off-diagonal terms are proportional to λ^{-1}, while $R_{22} \sim \lambda^{-2}$. As a consequence of this, near threshold the τ-approximation is insufficient, since there are diagrams not included in it which diverge for $\lambda \to 0$. For example, a simple estimate of the one-loop diagrams $\pi^{(1)}$ for the polarization operator (Fig. 6a) gives

$$\Pi_{02}^{(1)} \sim \Pi_{11}^{(1)} \propto \begin{pmatrix} \lambda^{-3+n/2} & \lambda^{-2+n/2} \\ \lambda^{-2+n/2} & 0 \end{pmatrix}, \tag{3.10}$$

where n is the spatial dimension of the system. In order to improve the τ-approximation it is necessary to extract the leading diagrams in $\lambda^{-\alpha}$ ($\alpha > 0$). We are therefore up against a problem, which at first glance rules out the possibility of our making such a choice in general. It turns out that if in the skeleton diagrams we substitute the functions d (2.3) and g (3.8) in the τ-approximation, the quantity α increases as we go to higher orders in perturbation theory. Thus, if we introduce the two new vertices (1.5) into a given diagram, there arise diagrams which, although having one extra integration $d\varepsilon d^n p$ (giving a small contribution in the anomalous region, whose volume goes as $\lambda^{1+n/2}$), also contain large coefficients of type $fg^{a(r)}$ which go as λ^{-3}. Because in the τ-approximation $d \sim$ constant in the anomalous region, the

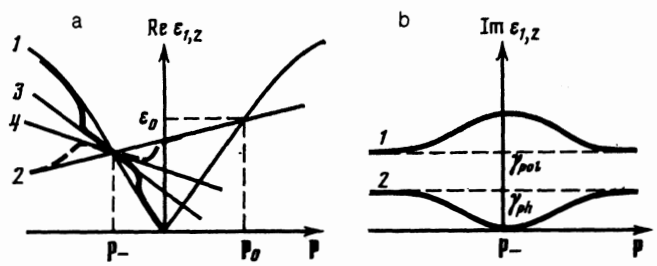

FIG. 9. (a) The dependence of $\operatorname{Re}\varepsilon_1(p)$ (curve 1) and $\operatorname{Re}\varepsilon_2$ (curve 2); (b) the same for $\operatorname{Im}\varepsilon_1(p)$ (curve 1) and $\operatorname{Im}\varepsilon_2(p)$ (curve 2). The straight lines 3 and 4 are projections onto the plane $p = 0$ of the tangent planes to the spectra at the point $\mathbf{p} = \mathbf{p}_-$.

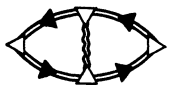

FIG. 10. The "correction" $\pi^{(2)}$ to the diagram $\pi^{(1)}$ in Fig. 6a, which is actually larger than the latter if in place of d and g we substitute their values in the τ-approximation.

magnitude of these diagrams is increased by a large factor $\lambda^{-2+n/2}$. For example, the components of the diagram $\pi^{(2)}$ in Fig. 10

$$\Pi_{02}^{(2)} \sim \Pi_{11}^{(2)} \propto \begin{pmatrix} \lambda^{-5+n} & \lambda^{-4+n} \\ \lambda^{-4+n} & 0 \end{pmatrix} \tag{3.11}$$

can be substantially larger than the components of the diagram for $\pi^{(1)}$ (Fig. 6a).

In this estimate, however, we have ignored the fact that to leading order in λ^{-1} the components of the function g are linear in the single function R. If we include in the polarization operator the large diagram $\pi^{(1)}$ (i.e., depart from the τ-approximation framework), this leads to mutual compensation of the leading terms in λ^{-1} for higher order diagrams, and these diagrams do not grow in size. We will demonstrate this by performing a certain linear transformation: let

$$x^{-1} = \begin{bmatrix} 2^{1/2}(\bar{\gamma}/\Gamma)I & 2^{1/2}i(\gamma_{pol}/\Gamma)\sigma_z \\ -2^{-1/2}i\sigma_z & -2^{-1/2}(\gamma_{ph}/\bar{\gamma})I \end{bmatrix},$$

$$x = \begin{bmatrix} 2^{-1/2}(\gamma_{ph}/\bar{\gamma})I & 2^{1/2}i(\gamma_{pol}/\Gamma)\sigma_z \\ -2^{-1/2}i\sigma_z & -2^{1/2}(\bar{\gamma}/\Gamma)I \end{bmatrix}, \tag{3.12}$$

where

$$x^{-1}x = xx^{-1} = \begin{bmatrix} I & 0 \\ 0 & I \end{bmatrix}, \quad I = \begin{pmatrix} 1 & 0 \\ 0 & 1 \end{pmatrix}.$$

It is easy to verify that for (3.8) the following relation holds

$$\tilde{g}(p) = x^{-1}g(p)x = \begin{bmatrix} R(p) & 0 \\ 0 & 0 \end{bmatrix}. \tag{3.13}$$

In addition, the vertices which transform according to the rule $\tilde{m}_{\alpha\beta}^{\gamma} = x_{\alpha\alpha'}^{-1} m_{\alpha'\beta'}^{\gamma} x_{\beta'\beta}$ take the form

$$\tilde{m}_{11}{}^{1} = -i(\bar{\gamma}/\Gamma)M\sigma_z, \quad \tilde{m}_{11}{}^{2} = i(\bar{\gamma}/\Gamma)\sigma_z M, \tag{3.14}$$

where, for example,

$$\|M\sigma_z\|_{ij}{}^{k} \equiv M_{ij'}^{k}(\sigma_z)_{j'j}.$$

(The vertices (3.14) are sufficient for us because only $\tilde{g}_{11} = R$ is non-zero).

Let us now include the single-loop diagrams $\pi^{(1)}$ in the polarization operator in addition to the term $\Pi^{(0)}$, i.e., (2.1). Then

$$\pi = \pi^{(0)} + \pi^{(1)} = \begin{bmatrix} -\sigma_z\Pi^{(1)} & \sigma_z(\Pi^{(0)}+\Pi^{(1)})\sigma_z \\ \Pi^{(0)}+\Pi^{(1)} & -\Pi^{(1)}\sigma_z \end{bmatrix}, \tag{3.15}$$

where the matrix

$$\|\Pi^{(1)}(p)\|_{ij} = \mu^2 \frac{\bar{\gamma}^2}{\Gamma^2} \int \frac{d^{n+1}q}{(2\pi)^{n+1}} \operatorname{Sp} \sigma_z M^i R(q) M^j \sigma_z R(q-p), \tag{3.16}$$

and the trace is taken over the omitted indices. Formula (3.15) shows in particular that to leading order in λ^{-1} a formula holds which is analogous to the Hugenholtz-Pines formula for a nonideal Bose gas:

$$\Pi_{11}{}^{a}\Pi_{11}{}^{r} - \Pi_{02}{}^{a}\Pi_{20}{}^{a} = 0. \tag{3.17}$$

The matrix (3.15) is diagonalized (in the "external" indices) with the help of the linear transformation

$$\tilde{\pi} = y^{-1}\pi y = \begin{bmatrix} \sigma_z\Pi^{(0)} & 0 \\ 0 & -(2\Pi^{(1)}+\Pi^{(0)})\sigma_z \end{bmatrix}, \tag{3.18}$$

where

$$y = 2^{-1/2}\begin{bmatrix} I & -\sigma_z \\ \sigma_z & I \end{bmatrix}, \quad y^{-1} = y^{\dagger}. \tag{3.19}$$

If we limit ourselves to terms linear in p for a small-$\mathbf{p}$ expansion of $\varepsilon_0(\mathbf{p})$, then $\varepsilon_0(\mathbf{p}) = -\varepsilon_0(-\mathbf{p})$ and

$$d_0 = \begin{bmatrix} 0 & D_0 \\ \sigma_z D_0 \sigma_z & 0 \end{bmatrix}. \tag{3.20}$$

This matrix is diagonalized in the "external" indices by the transformation $\tilde{d}_0 = y^{-1}d_0 y$. Therefore, the solution to (1.17) is also diagonalized and takes the form

$$\tilde{d} = (\tilde{d}_0{}^{-1} - \tilde{\pi})^{-1} = \begin{bmatrix} D_1\sigma_z & 0 \\ 0 & -\sigma_z D_2 \end{bmatrix}, \tag{3.21}$$

where D_1 coincides with the solution to 2.3 in the τ-approximation, while

$$D_2 = \begin{pmatrix} 0 & (D_0^{-1} - \Pi^{(0)a} - 2\Pi^{(1)a})^{-1} \\ (D_0^{-1} - \Pi^{(0)r} - 2\Pi^{(1)r})^{-1} & (\Delta^{(0)} + 2\Delta^{(1)})\,|D_0^{-1} - \Pi^{(0)a} - 2\Pi^{(1)a}|^{-2} \end{pmatrix}. \tag{3.22}$$

For $\lambda \ll 1$ the operator $\Pi^{(1)}$ is the same order as (3.10) and $\Pi^{(1)} \gg \Pi^{(0)}$. Thus, in the anomalous region,

$$D_1 \propto \text{const}, \quad D_2 \propto \begin{pmatrix} 0 & \lambda^{2-n/2} \\ \lambda^{2-n/2} & \lambda^{1-n/2} \end{pmatrix}. \tag{3.23}$$

On the other hand, the transformed vertices $\tilde{m}_{\alpha\beta}{}^{\gamma} = \tilde{m}_{\alpha\beta}{}^{\gamma'} y_{\gamma'\gamma}$ take the form

$$\tilde{\tilde{m}}_{11}{}^{1} = 0, \quad \tilde{\tilde{m}}_{11}{}^{2} = 2^{1/2}i(\bar{\gamma}/\Gamma)\sigma_z M. \tag{3.24}$$

From this it is clear that the large functions R are connected through the vertices not with the finite D_1 but with the functions D_2. It is not difficult to show that the orders of the quantities D_2 are such that the addition of the new vertices to any diagram preserves its order in an expansion in powers of λ^{-1}.

4. MODEL SYSTEM

In the previous paragraph, it was shown that near threshold the τ-approximation is inapplicable, but that in principle it can be improved by a judicious choice of leading diagrams. Below we will construct a self-consistent approximation which takes into account one-loop diagrams in the

polarization operators. So as to simplify the problem, we will investigate a model system in which quanta of the coherent mode can decay into two quanta within the same free-particle spectrum.[4] Apparently, such a simplification is not too critical, since near threshold, as we have seen, even in the three-quanta problem the propagators for phonons and scattered polaritons coincide to within a numerical factor. A further simplification occurs because we are investigating only a one-dimensional system (for example, a polariton wave in a light fiber).

Dropping the subscripts pol and ph, we denote the components of the functions g and g_0 in the following way:

$$g=\begin{bmatrix} G & G_\lozenge \\ \bar{G}_\times & \bar{G}^{\mathrm{T}} \end{bmatrix}, \quad g_0=\begin{bmatrix} G_0 & 0 \\ 0 & \bar{G}_0^{\mathrm{T}} \end{bmatrix}. \tag{4.1}$$

Correspondingly, we transform also the matrix σ (1.14):

$$\sigma=\begin{bmatrix} \Sigma_{11} & \Sigma_{02} \\ \bar{\Sigma}_{20} & \bar{\Sigma}_{11}^{\mathrm{T}} \end{bmatrix}. \tag{4.2}$$

Including in the expansions of the spectra around the special points only leading terms linear in p (here p is a one-dimensional vector), we will use the following forms for the free-particle Green's functions:

$$G_0^{-1}(p)=(\varepsilon+wp)\sigma_z, \quad D_0^{-1}(p)=(\varepsilon-vp)\sigma_z. \tag{4.3}$$

It is easy to show that for each of the functions g, d, σ and π only two of the four matrix components are linearly independent; for these functions, the following relations hold:

$$g=\begin{bmatrix} G & G_\lozenge \\ -\sigma_z G_\lozenge \sigma_z & \sigma_z G \sigma_z \end{bmatrix}, \quad \sigma=\begin{bmatrix} \Sigma_{11} & \Sigma_{02} \\ -\sigma_z\Sigma_{02}\sigma_z & \sigma_z\Sigma_{11}\sigma_z \end{bmatrix}, \tag{4.4}$$

$$d=\begin{bmatrix} D_\lozenge & D \\ \sigma_z D \sigma_z & \sigma_z D_\lozenge \sigma_z \end{bmatrix}, \quad \pi=\begin{bmatrix} \sigma_z\Pi_{02}\sigma_z & \sigma_z\Pi_{11}\sigma_z \\ \Pi_{11} & \Pi_{02} \end{bmatrix}. \tag{4.5}$$

The differences in sign between (4.4) and (4.5) are related to the fact that diagrams for G, $\Sigma_\parallel$, D, $\Pi_\parallel$, D_x and Π_{02} contain an even number of the vertices (1.7), while those for G_x and Σ_{02} contain an odd number.

The matrices (4.4) and (4.5) are diagonalized in the external indices with the help of the transformations (3.12) and (3.19). In the matrix (3.12) we must set $\gamma_{\mathrm{ph}}=\gamma_{\mathrm{pol}}$:

$$x=x^{-1}=2^{-1/2}\begin{bmatrix} I & i\sigma_z \\ -i\sigma_z & I \end{bmatrix}. \tag{4.6}$$

Then

$$\tilde{g}_0=x^{-1}g_0x=\begin{bmatrix} G_0 & 0 \\ 0 & \sigma_z G_0 \sigma_z \end{bmatrix}, \quad \tilde{d}_0=y^{-1}d_0y=\begin{bmatrix} D_0\sigma_z & 0 \\ 0 & -\sigma_z D_0 \end{bmatrix}, \tag{4.7}$$

$$\tilde{g}=x^{-1}gx$$

$$=\begin{bmatrix} G-iG_\lozenge\sigma_z & 0 \\ 0 & \sigma_z(G+iG_\lozenge\sigma_z)\sigma_z \end{bmatrix}\equiv\begin{bmatrix} G_1 & 0 \\ 0 & \sigma_z G_2 \sigma_z \end{bmatrix}, \tag{4.8}$$

$$\tilde{d}=y^{-1}dy=\begin{bmatrix} (D+D_\lozenge\sigma_z)\sigma_z & 0 \\ 0 & -\sigma_z(D-D_\lozenge\sigma_z) \end{bmatrix}$$

$$\equiv\begin{bmatrix} D_1\sigma_z & 0 \\ 0 & -\sigma_z D_2 \end{bmatrix}, \tag{4.9}$$

$$\tilde{\sigma}=x^{-1}\sigma x$$

$$=\begin{bmatrix} \Sigma_{11}-i\Sigma_{02} & 0 \\ 0 & \sigma_z(\Sigma_{11}+i\Sigma_{02})\sigma_z \end{bmatrix}\equiv\begin{bmatrix} \Sigma_1 & 0 \\ 0 & \sigma_z\Sigma_2\sigma_z \end{bmatrix}, \tag{4.10}$$

$$\tilde{\pi}=y^{-1}\pi y=\begin{bmatrix} \sigma_z(\Pi_{11}+\Pi_{02}\sigma_z) & 0 \\ 0 & -(\Pi_{11}-\Pi_{02}\sigma_z)\sigma_z \end{bmatrix}$$

$$=\begin{bmatrix} \sigma_z\Pi_1 & 0 \\ 0 & -\sigma_z\Pi_2 \end{bmatrix} \tag{4.11}$$

$$\tilde{\Phi}=x^{-1}\Phi x=\begin{bmatrix} -\Phi\sigma_y & 0 \\ 0 & \Phi\sigma_z\sigma_y\sigma_z \end{bmatrix}. \tag{4.12}$$

The vertices, which transform according to the rule $\tilde{m}^\alpha_{\beta\gamma}=x_{\beta\beta'}\,m^{\alpha'}_{\beta'\gamma'}x_{\gamma'\gamma}y_{\alpha'\alpha}$ have four non-zero components

$$\tilde{m}_{11}{}^2=2^{-1/2}i\sigma_z M, \quad \tilde{m}_{22}{}^2=-2^{-1/2}iM\sigma_z,$$

$$\tilde{m}_{12}{}^1=-2^{-1/2}M, \quad \tilde{m}_{21}{}^1=-2^{-1/2}\sigma_z M\sigma_z. \tag{4.13}$$

After the diagonalization equations (1.16) and (1.17) are easily solved. The functions $G_{1,2}$ and $D_{1,2}$ which enter into the solutions [see (4.8), (4.9)] have the form

$$G_{1,2}(p)$$

$$=\begin{pmatrix} 0 & [\varepsilon+wp-\Sigma^a_{1,2}(p)\pm i\Phi]^{-1} \\ [\varepsilon+wp-\Sigma^r_{1,2}(p)\mp i\Phi]^{-1} & \Omega_{1,2}|\varepsilon+wp-\Sigma^a_{1,2}\pm i\Phi|^{-2} \end{pmatrix} \tag{4.14}$$

(the upper sign refers to the function G_1) and

$$D_{1,2}(p)=\begin{pmatrix} 0 & [\varepsilon-vp-\Pi^a_{1,2}(p)]^{-1} \\ [\varepsilon-vp-\Pi^r_{1,2}(p)]^{-1} & \Delta_{1,2}|\varepsilon-vp-\Pi^a_{1,2}|^{-2} \end{pmatrix}. \tag{4.15}$$

5. THE MODEL SYSTEM NEAR THRESHOLD

Let us first investigate the τ-approximation, in which

$$\Sigma_{02}=0, \quad \Sigma_{11}=i\gamma_0\begin{pmatrix} -2 & -1 \\ 1 & 0 \end{pmatrix}, \tag{5.1}$$

where γ_0 is the decay constant for g-particles in zero field. Then

$$G_{1,2}$$

$$=\begin{pmatrix} 0 & [\varepsilon+wp-i(\gamma_0\mp\Phi)]^{-1} \\ [\varepsilon+wp+i(\gamma_0\mp\Phi)]^{-1} & -2i\gamma_0[(\varepsilon+wp)^2+(\gamma_0\mp\Phi)^2]^{-1} \end{pmatrix}. \tag{5.2}$$

In the τ-approximation, therefore, the threshold for generation is reached when $\Phi_c=\gamma_0$. Near threshold, for $\Phi=\gamma_0(1-\lambda)$, $\lambda\ll 1$, the components of the function $\tilde{g}_{11}=G_1$ are large, whereas the component function G_2 is finite (compare with (3.13), taking into account only the leading terms in λ^{-1}).

We now investigate the possibility of generating g-quanta outside the framework of the τ-approximation, i.e., when Σ_1 and Σ_2 are certain functions of Φ. We denote

$$\mathrm{Im}\,\Sigma^a_{1,2}(p,\Phi)\equiv\gamma_{1,2}(p,\Phi).$$

From (4.14) it is clear that for $\Phi\sim\Phi_c$, where Φ_c is a root of the equation

$$\gamma_1(0,\Phi)-\Phi=0, \tag{5.3}$$

the imaginary part of the denominator of G_1 is small and changes sign as Φ passes through Φ_c. Therefore, if there is a solution to (5.3), it corresponds to the threshold for generation of g-quanta. Let us assume that such a Φ_c exists (we will verify this *a posteriori*). As in section 3, we will study the system behavior below threshold but close to the threshold region. Let

$$\Phi_c-\Phi\equiv\lambda\Phi_c \tag{5.4}$$

where the quantity $\lambda\ll 1$ is a parameter which determines how we will select our diagrams.

If $\gamma_1(\Phi)$ is differentiable for $\Phi\sim\Phi_c$, then for small p and $\Phi\sim\Phi_c$, analogous to (3.3) we have

$$\gamma_1\approx\Phi_c-(\partial\gamma_1/\partial\Phi)_{\Phi=\Phi_c}\lambda\Phi_c+ap^2,\quad a\sim w^2/\gamma_0.$$

Therefore

$$(\gamma_1-\Phi)_{\Phi=\Phi_c(1-\lambda)}\approx\lambda\Psi_c+ap^2, \tag{5.5}$$

where

$$\Psi_c=[1-(\partial\gamma_1/\partial\Phi)_{\Phi=\Phi_c}]\Phi_c. \tag{5.6}$$

For $|\varepsilon|\lesssim\lambda\Psi_c$, $|\mathbf{p}|\lesssim\lambda^{1/2}\Psi_c/w$, the functions $G_{1,2}$ can be cast in the form

$$G_1(p)\approx\begin{pmatrix}0 & [\varepsilon+w\mathbf{p}-i(\lambda\Psi_c+ap^2)]^{-1}\\ [\varepsilon+w\mathbf{p}+i(\lambda\Psi_c+ap^2)]^{-1} & -i\alpha_1[(\varepsilon+w\mathbf{p})^2+(\lambda\Psi_c+ap^2)^2]^{-1}\end{pmatrix}, \tag{5.7}$$

$$G_2(p)\approx\begin{pmatrix}0 & [\varepsilon+w\mathbf{p}-i(\gamma_2+\Phi_c)]^{-1}\\ [\varepsilon+w\mathbf{p}+i(\gamma_2+\Phi_c)]^{-1} & -i\alpha_2[(\varepsilon+w\mathbf{p})^2+(\gamma_2+\Phi_c)^2]^{-1}\end{pmatrix}, \tag{5.8}$$

where

$$-i\alpha_{1,2}\equiv\Omega_{1,2}(0),\quad i\gamma_2=\Sigma_2^a(0). \tag{5.9}$$

Here it is assumed that the functions $\Omega_{1,2}(p)$ and $\Sigma_{1,2}(p)$ are analytic for $\Phi\sim\Phi_c$, $p\sim 0$. This assumption can be proved within the framework of the self-consistent approximation to be developed below.

The goal of the next investigation is to find self-consistent values for Φ_c, $\alpha_{1,2}$, γ_2, $(\partial\gamma_1/\partial\Phi)_{\Phi=\Phi_c}$. The single-loop diagrams for the polarization operators included in the self-consistent approximation are representative in order of magnitude (see section 3). But higher-order diagrams, generally speaking, will also be of the same order in an expansion of λ^{-1}. The situation near threshold, consequently, coincides with the situation near a phase transition, and a full solution requires the use of the renormalization group. We will not solve this problem here, but rather limit ourselves to the mean-field approximation.

6. SELF-CONSISTENT APPROXIMATION

Let us first calculate the polarization operator (Fig. 6a), using the representations (5.7) and (5.8) for the functions $G_{1,2}$ in terms of the parameters Φ_c, $\alpha_{1,2}$, ... In addition, by making use of (4.15), we obtain also the function d. After then calculating $\tilde{\sigma}$ (Fig. 6b), we will compare the expressions we derive with (5.6), (5.9), and thereby obtain the self-consistency equation. The solutions to these equations in terms of the parameters Φ_c, $\alpha_{1,2}$ are presented in the following Table I:

TABLE I.

	$\frac{\Phi_c}{\gamma_0}$	$\frac{\alpha_1}{\gamma_0}$	$\frac{\partial\gamma_1}{\partial\Phi}\Big\vert_{\Phi_c}$	$\frac{\alpha_2}{\gamma_0}$	$\frac{\gamma_2}{\gamma_0}$
τ-approximation	1	2	0	2	1
Self-consistent approx.	1	8	−1	4	3

For comparison, we also present the values of these parameters within the τ-approximation (see section 5). In the self-consistent approximation, as is clear from Table I, a linear dependence on the field amplitude appears in the decay constant near threshold, and the occupation numbers are also renormalized. Thus, the functional form of the propagators for scattered polaritons and phonons is not changed. The fact that the value of the amplitude Φ_c is the same for both approximations is related to the neglect of the dependences of g and d on p (within the framework of the self-consistent approximation) for large p. The most significant disagreement between the two approximations is in their description of the particles with $p\sim p_0$ [compare (2.3) with (4.9) and (4.15); the expressions for the operators $\Pi_{1,2}$ in (4.15) are presented below, see (6.3), (6.4), (6.6) and (6.7)]. In the self-consistent approximation, near the coherent wave there appears a low-intensity but broad-spectrum noise amplitude.

We now turn to a description of the self-consistent approximation.[5)]

A. Polarization operator $\tilde{\Pi}$

Let us calculate the operator $\Pi_1(q)=\sigma_z\tilde{\pi}_{11}(q)$, $q=(\omega,\mathbf{q})$ (see (4.11) and Fig. 11a). Using (4.8) and (4.13), we obtain

$$\Delta_1(q)=i\mu^2\int\frac{d\varepsilon\,d\mathbf{p}}{(2\pi)^2}[F_1(p)F_2(p-q)-G_1^a(p)G_2^r(p-q)-G_1^r(p)G_2^a(p-q)], \tag{6.1}$$

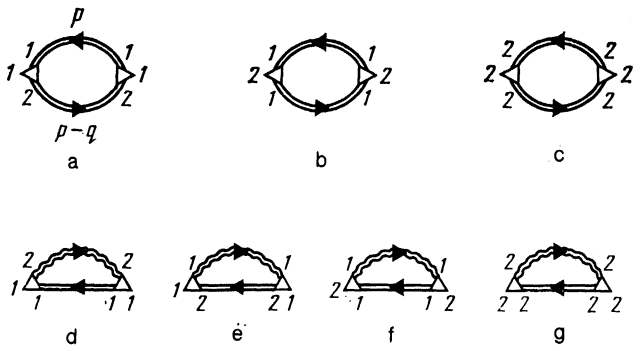

FIG. 11. One-loop diagrams for $\tilde{\pi}_{11}$(a), $\tilde{\pi}_{22}$ (b, c), $\tilde{\sigma}_{11}$ (d, e) and $\tilde{\sigma}_{22}$ (f, g). Here, the numbers are "external" indices.

$$\Pi_1^r(q)=-i\mu^2\int\frac{d\varepsilon\,d\mathbf{p}}{(2\pi)^2}[F_1(p)G_2^a(p-q)-G_1^r(p)F_2(p-q)]. \tag{6.2}$$

The leading terms in (6.1) and (6.2) equal

$$\Delta_1(q)\approx\frac{-i\mu^2\alpha_1\alpha_2}{4a^{1/2}[(\omega+wq)^2+(\Phi_c+\gamma_2)^2]}(\lambda\Psi_c)^{-1/2}, \tag{6.3}$$

$$\Pi_1^r(q)\approx\frac{\mu^2\alpha_1}{4a^{1/2}[\omega+wq+i(\Phi_c+\gamma_2)]}(\lambda\Psi_c)^{-1/2}. \tag{6.4}$$

We note that Π_1 is slowly-varying in the vicinity of $q=0$. With the help of (4.15) we find that over a wide interval of values $|\omega|\lesssim\Phi_c$, $|\mathbf{q}|\lesssim\Phi_c/\omega$

$$D_1(q)\approx D_1(0)$$

$$\approx\frac{4(\lambda\Psi_c a)^{1/2}(\Phi_c+\gamma_2)}{\alpha_1\mu^2}\begin{pmatrix}0 & i\\ -i & -i\alpha_2/(\Phi_c+\gamma_2)\end{pmatrix}. \tag{6.5}$$

We now calculate $\Pi_2(q)=-\tilde{\pi}_{22}(q)\sigma_z$ (Figs. 11b and 11c). The basic contribution to Π_2 comes from the integration over the anomalous region involved in the diagram in Fig. 11b:

$$\Pi_2^r(q)\approx-i\mu^2\int\frac{d\varepsilon\,d\mathbf{p}}{(2\pi)^2}F_1(p)G_1^a(p-q)=-iA\lambda^{-1/2}Q^r(\eta,\xi), \tag{6.6}$$

$$\Delta_2(q)\approx\frac{i\mu^2}{2}\int\frac{d\varepsilon\,d\mathbf{p}}{(2\pi)^2}[F_1(p)F_1(p-q)-G_1^aG_1^r-G_1^rG_1^a]$$

$$=-iB\lambda^{-1/2}2\,\mathrm{Re}\,P(\eta,\xi), \tag{6.7}$$

where

$$\eta=\frac{\omega+wq}{\lambda\Psi_c},\quad \xi=\left(\frac{a}{\lambda\Psi_c}\right)^{1/2}q,\quad A=\frac{\mu^2\alpha_1}{8\Psi_c(a\Psi_c)^{1/2}},$$

$$B=\frac{\mu^2\alpha_1^2}{32\Psi_c^2(a\Psi_c)^{1/2}},$$

$$Q^r(\eta,\xi)=i\{(\xi+i\xi^2/2+\eta/2)^{-1}-[\xi(1+\xi^2/4-i\eta/2)^{1/2}+\eta/2]^{-1}(1+\xi^2/4-i\eta/2)^{-1/2}\}, \tag{6.8}$$

$$P(\eta,\xi)=[(\xi^2/2+i\xi)^2+\eta^2/4]^{-1}+[\xi^2(1+\xi^2/4-i\eta/2)-\eta^2/4]^{-1}(1+\xi^2/4-i\eta/2)^{-1/2}. \tag{6.9}$$

In contrast to Π_1, the operator Π_2 is strongly dependent on q in the neighborhood of $q=0$.

B. Polarization operator $\tilde{\sigma}$

Let us calculate the matrix component $\approx -i(\Phi_c+\gamma_2)/2$. (Figs. 11d, 11e). The diagram shown in Fig. 11d makes the following contribution to $\Omega_1(0)$:

$$\frac{i\mu^2}{2}\int\frac{d\varepsilon\,d\mathbf{p}}{(2\pi)^2}[F_1(p)S_2(p)+G_1^aD_2^r+G_1^rD_2^a]. \tag{6.10}$$

It can be shown that after integrating over the anomalous region the basic contribution to (6.10), which is finite as $\lambda\to0$ and equal to $-3i\alpha_1/4$, comes from the first term. The integral for large p, where the function under the integral differs only slightly from the $\Phi=0$ function, together with the diagram in Fig. 11e, gives $-2i\gamma_0$. Consequently, the self-consistent value of α_1 is found from the relation

$$-i\alpha_1=\Omega_1(0)\approx-{}^3/_4i\alpha_1-2i\gamma_0 \tag{6.11}$$

and so $\alpha_1\approx+8\gamma_0$.

Let us now calculate $\Sigma_1^r(0)$. The diagram in Fig. 11d gives

$$-\frac{i\mu^2}{2}\int\frac{d\varepsilon\,d\mathbf{p}}{(2\pi)^2}[F_1(p)D_2^a(p)+G_1^r(p)S_2(p)]. \tag{6.12}$$

It can be shown that the integral in (6.12) over the anomalous region gives only a small contribution, proportional to λ and equal to $-i\lambda\Psi_cK$. Numerical calculations give $K\approx0.5$. On the other hand, the integral in (6.12) for large p, together with the diagram in Fig. 11e, gives a finite contribution as $\lambda\to0$ which equals $-i\gamma_0$. Thus, this self-consistency condition takes the form

$$-i\gamma_1|_{\Phi=\Phi_c(1-\lambda)}=\Sigma_1^r(0)=-i\gamma_0-iK\lambda\Psi_c. \tag{6.13}$$

From this, using (5.5) and (5.6), we obtain

$$\Phi_c=\gamma_0,\qquad(\partial\gamma_1/\partial\Phi)_{\Phi=\Phi_c}=K/(K-1)\approx-1. \tag{6.14}$$

It remains to calculate the matrix component $\Sigma_2(0)=\sigma_z\tilde{\sigma}_{22}\sigma_z$ (Figs. 11f, 11g). The diagram in Fig. 11f gives the following contribution to $\Omega_2(0)$:

$$\frac{i\mu^2}{2}\int\frac{d\varepsilon\,d\mathbf{p}}{(2\pi)^2}[F_1(p)S_1(p)+G_1^aD_1^r+G_1^rD_1^a]. \tag{6.15}$$

The basic contribution to (6.15), which is finite as $\lambda\to0$ and equal to $-i\alpha_2/2$, is contained in the first term. The large-p integral for both the diagrams 11f and 11g gives $-2i\gamma_0$. Thus, the self-consistency condition for α_2 takes the form

$$-i\alpha_2=\Omega_2(0)\approx-i\alpha_2/2-2i\gamma_0, \tag{6.16}$$

or $\alpha_2\approx4\gamma_0$.

Diagram 11d for $\Sigma_2^r(0)$ gives

$$\frac{i\mu^2}{2}\int\frac{d\varepsilon\,d\mathbf{p}}{(2\pi)^2}[F_1(p)D_1^a(p)+G_1^rS_1]. \tag{6.17}$$

The first term in (6.17) integrated over the anomalous region gives a finite contribution as $\lambda\to0$, equal to $\approx-i(\Phi_c+\gamma_2)/2$. Including the large-$p$ contribution to the integral, we obtain the self-consistency condition for γ_2:

$$-i\gamma_2=\Sigma_2(0)\approx-i(\Phi_c+\gamma_2)/2-i\gamma_0, \tag{6.18}$$

i.e., $\gamma_2\approx3\gamma_0$.

CONCLUSION

Let us discuss the applicability of the model we have just investigated to a real polariton system in an optical fiber. In order to use the one-dimensional model, it is necessary that only light waves with $p_\perp = 0$ propagate. Transverse modes will not be excited if the spacing (in frequency) between them satisfies $\Delta\omega \sim W/l$ (where W is the phase velocity of the wave and l is the thickness of the fiber) exceeds the spectral width γ_0. This can be achieved if we take a thin enough fiber, i.e., with $l \ll W/\gamma_0$.

In order to apply the self-consistent approximation, we had to show first that the one-loop polarization operators Π_1 (6.3), (6.4) and Π_2 (6.6)–(6.9) were large compared to the τ-approximation polarization operators

$$\Pi_1 \gg \Pi^{(0)}, \quad \Pi_2 \gg \Pi^{(0)}, \tag{7.1}$$

and second, that the higher-order diagrams in perturbation theory were small compared to $\Pi_{1,2}$. It is easy to show that in order of magnitude

$$\Pi_1 \sim \Lambda\lambda^{-1/2}\Pi^{(0)}, \quad \Pi_2 \sim \gamma_0\Lambda\begin{pmatrix} \lambda^{-5/3} & \lambda^{-3/2} \\ \lambda^{-3/2} & 0 \end{pmatrix}. \tag{7.2}$$

Here, the dimensionless quantity $\Lambda = \mu^2/\omega\gamma_0 < 1$, since the scattering of polaritons by phonons, which gives (as is not difficult to show) a contribution to the polariton width on the order of μ^2/w[6] is not solely due to the broadening of the polariton levels. There are also in γ_0 contributions from interactions with optical phonons, impurity scattering, and losses at the surfaces of the optical fiber. The scale of nearness to the threshold for stimulated scattering is naturally determined by powers of Λ, which also define the regions I–IV shown in Fig. 12 in which various relations hold between the polarization operators $\Pi_{1,2}$ and $\Pi^{(0)}$. In region I the τ-approximation holds; in region IV the self-consistent approximation holds. In regions II and III, some of the parameters are determined by the τ-approximation while others are determined within the self-consistent scheme.

For the self-consistent approximation, the situation is worse as regards fulfilling the second applicability condition, since as we have already pointed out all the higher-order perturbation diagrams are, generally speaking, of the same order as $\Pi_{1,2}$. The analogous situation arises in the theory of phase transitions; a full solution to the problem requires the use of the renormalization group.

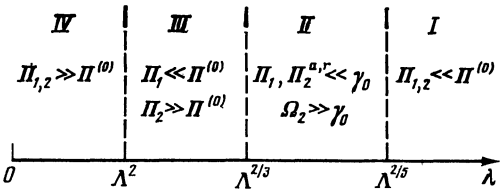

FIG. 12. Ranges of λ over which various inequalities hold between the components Π_1, Π_2, and $\Pi^{(0)}$.

Finally, let us discuss the region of applicability of the undepleted (i.e., prescribed pump approximation. It is not hard to show that the total spatial density of polaritons after scattering near threshold

$$n_- \sim n_c\Lambda\lambda^{-1/2}. \tag{7.3}$$

Consequently, the undepleted pump approximation obtains in regions I–III (Fig. 12) and does not hold near threshold in region IV, where losses to scattering become significant. (The intensity of polaritons before scattering in the framework of the self-consistent approximation is found to be small compared to n_c for all λ.)

[1)]We use the index notation from Ref. 4.
[2)]In this case, for calculating $z^{1/2}$ it is convenient to put the cut along the line $\mathrm{Im}\, z = 0$, $\mathrm{Re}\, z > 0$.
[3)]We will call this small region around $p = 0$ the "anomalous" region.
[4)]However, we will not assume these two quanta are identical particles in the quantum-mechanical senses. For this reason, the model developed below cannot be directly applied to problems such as the decay of optical phonons into acoustic phonons.
[5)]A similar calculation was presented in Ref. 7.
[6)]In the one-dimensional case, in determining the vertex (1.6), in place of a volume density ρ a line density down the optical fiber of ρl^2. Thus, the dimensions of $[\mu^2/w]$ are s^{-1}.

[1]A. L. Ivanov and L. V. Keldysh, Zh. Eksp. Teor. Fiz. **84**, 404 (1983) [Sov. Phys. JETP **57**, 234 (1983)].
[2]Eksitony (Excitons; Eds. E. I. Rashba and M. D. Stredzha). M.: Nauka, Chs. 2,3.
[3]L. V. Keldysh, Zh. Eksp. Teor. Fiz. **47**, 1515 (1964) [Sov. Phys. JETP **20**, 1018 (1964)].
[4]S. T. Beliaev, Zh. Eksp. Teor. Fiz. **34**, 417 (1958) [Sov. Phys. JETP **7**, 289 (1958)]; Zh. Eksp. Teor. Fiz. **34**, 433 (1958) [Sov. Phys. JETP **7**, 299 (1958)].
[5]I. B. Levinson, Zh. Eksp. Teor. Fiz. **65**, 331 (1973) [Sov. Phys. JETP **38**, 162 (1973)].
[6]N. Hugenholtz and D. Pines, Phys. Rev. **116**, 489 (1959).
[7]L. V. Keldysh and S. G. Tikhodeev, FIAN No. 331 (1985) (Preprint).

Translated by F. J. Crowne